Scanning Electron Microscopy

Volume 1985
Number 2 *Part II*

Article 13

5-20-1985

The Ballistic Phonon Signal in Low Temperature Scanning Electron Microscopy

R. P. Huebener
Universität Tübingen

W. Metzger
Universität Tübingen

SCANNING ELECTRON MICROSCOPY/1985/II (Pages 617-626)
SEM Inc., AMF O'Hare (Chicago), IL 60666 USA

0586-5581/85$1.00+.05

THE BALLISTIC PHONON SIGNAL IN LOW TEMPERATURE SCANNING ELECTRON MICROSCOPY

R. P. Huebener* and W. Metzger

Physikalisches Institut II, Universität Tübingen
D - 7400 Tübingen, FRG

(Paper received November 30 1984, Completed manuscript received May 20 1985)

Abstract

By scanning the surface of a specimen cooled to liquid-helium temperature with the electron beam, ballistic phonons are generated which can be used for acoustic imaging. The anisotropy of the ballistic phonon propagation caused by the phonon focusing effect has been observed in recent experiments. The simultaneous operation of two or more small-area phonon detectors during the scanning process appears promising for three-dimensional acoustic imaging of structural inhomogeneities even far from the specimen surface. The principles of this scheme for acoustic imaging are discussed and the spatial resolution limits are estimated.

KEY WORDS: Scanning electron microscopy, low-temperature stage, ballistic phonon signal, Planck's radiation law, phonon focusing, acoustic tomography, bolometer

*Address for correspondence:
R. P. Huebener, Physikalisches
Institut II, Universität Tübingen,
Morgenstelle 14, D - 7400 Tübingen 1, FRG
Phone No. (07071) 296315

Introduction

In scanning microscopy various schemes for imaging utilizing acoustic signals have recently been developed or proposed. On the one hand, a beam modulated at high frequencies can serve for generating an acoustic wave, its frequency being identical to the modulation frequency of the beam. Here the modulated thermal expansion near the sample surface at the point of the beam focus represents perhaps the most important mechanism for generating the acoustic signal. On the other hand, the region locally heated by the beam can emit quanta of sound energy (phonons), similar to the emission of quanta of visible light from the heated filament in a light bulb. The quanta of sound energy propagate at sound velocity through the crystal, and they are scattered or absorbed by structural inhomogeneities in the sample. Both schemes can be realized using either an electron beam or a light beam (laser) for scanning the surface of the specimen. Whereas in the first scheme the acoustic imaging is restricted to a region close to the sample surface, in the second scheme acoustic images can also be obtained from spatial structures in the interior of the specimen. In the latter case the depth for acoustic imaging is limited by the mean free path of the phonons propagating through the specimen. For this reason, in this case it is advantageous to cool the sample to low temperatures during the acoustic imaging process, since at low temperatures the phonon mean free path is relatively large.

In this paper we first briefly summarize the essential aspects of the acoustic imaging process based on the generation of acoustic waves with the same frequency as the frequency of the beam modulation. Then we discuss in detail the main features of acoustic imaging based on the emission of acoustic phonons from the region locally heated by the beam. Here space- and time-resolved phonon detection will be seen to become crucial. Recent experiments on phonon focusing, in which this technique has been employed, are summarized. Further, the possibilities for three-dimensional acoustic imaging of structural inhomogeneities in the sample interior will be outlined. Finally, the resolution limits of this acoustic imaging technique are estimated.

Scanning Electron-Acoustic and Photoacoustic Microscopy

The principle of scanning electron acoustic or photoacoustic microscopy is shown schematically in Fig. 1. A localized region at the specimen surface is heated periodically with an electron beam or a laser-beam the intensity of which is modulated at the angular frequency ω. In this region an acoustic wave is generated. It represents the signal to be detected. The frequency of this acoustic wave is identical to the modulation frequency ω. By scanning the beam over the specimen surface, the location of the thermal excitation can be shifted accordingly. The periodic heating results in the generation of a thermal wave. The radius η of the region showing a temperature modulation is approximately given by

$$\eta = \left(\frac{2\kappa}{\omega}\right)^{1/2} \qquad (1)$$

Here κ is the thermal diffusion constant:

$$\kappa = \frac{k}{\rho \cdot C} \qquad (2)$$

where k, ρ, and C are the heat conductivity, the mass density, and the specific heat of the irradiated material, respectively. For a typical metal at room temperature and a frequency $\nu = \frac{\omega}{2\pi} = 10\text{MHz}$ one finds from Eqs. (1) and (2) $\eta \approx 1$ µm. Typically, the modulation frequencies $\nu = \frac{\omega}{2\pi}$ range between 100 kHz and 100 MHz.

At present, the details of the mechanism for generating the acoustic wave by means of the modulated beam irradiation have not yet been clarified completely. However, it appears that thermoelastic expansion often plays a dominant role. In this case the acoustic wave contains information regarding the variation of the thermal and elastic properties within the heated region across the sample surface. Of course, the structural information obtained in this way is restricted to a region of thickness η close to the sample surface.

For detection of the acoustic signal two principles have been employed, which are shown schematically in Fig. 2. In one case, the sample is placed in a small gas cell and the pressure modulation in the gas resulting from the modulated beam irradiation is detected by a microphone. In another case, the acoustic wave is detected with a piezo-electric transducer attached to the sample.

For scanning the sample surface, an electron beam or a light beam (laser) can be used, resulting in what is called scanning electron-acoustic microscopy (SEAM) and scanning photo-acoustic microscopy (SPAM), respectively.

For a more detailed discussion of the principles and applications of scanning electron acoustic and photoacoustic microscopy see papers by Cargill [4, and private communication], Rosencwaig [12], Wong [15], Luukkala [8], and Balk [2]. Besides the acoustic signal generated at the frequency identical to that of the beam modulation, the signal at some harmonic frequencies have also been utilized for imaging [3]. In addition to utilizing the acoustic signal generated by the modulated beam irradiation, the local temperature rise at the sample surface, effected by a laser beam, has been recorded by means of the emitted infrared radiation detected as a function of the coordinates of the beam focus for obtaining structural information [Luukkala, private communication].

It is interesting to replace the heat conductivity k in Eq. (2) by the expression:

$$k = \frac{1}{3} \rho \cdot C \cdot v \cdot l \qquad (3)$$

obtained from kinetic theory. Here v and l are the velocity and the mean free path, respectively, of the particles accounting for the thermal properties of the specimen. If the electronic influence dominates, v must be identified with the Fermi velocity v_F and l with the mean free path l_e of the electrons. If the influence of the phonons dominates (as in an electric insulator), v must be identified with the sound velocity v_s and l with the mean free path l_{ph} of the phonons. Inserting Eq. (3) into Eq. (1), we obtain:

$$\eta = \left(\frac{2}{3} \frac{v \cdot l}{\omega}\right)^{1/2} \qquad (4)$$

We see that the length η, which determines the spatial resolution limit of scanning electron acoustic and photoacoustic microscopy, depends upon the mean free path of the electrons or the phonons in the specimen. This dependence upon the mean free path l will become important in our discussion below regarding the possible extension of acoustic imaging to the low-temperature regime.

Emission of Quanta of Sound Energy

The principle of scanning electron acoustic and photoacoustic microscopy discussed in the last section utilizes the acoustic wave generated by the specimen at the same frequency as the modulation frequency of the beam irradiation. Now we will turn to a different acoustic signal emanating from the region heated by the electron beam or the laser beam, namely the emitted quanta of sound energy propagating through the specimen at sound velocity. These emitted "particles" are usually referred to as ballistic phonons. This emission process is similar to the emission of quanta of visible light from matter at sufficiently high temperatures (heated filament in a light bulb).

In order to utilize the ballistic phonons for acoustic imaging, a long flight path of the phonons (phonon mean free path) without interruption by scattering or absorption represents a distinct advantage. Because of this reason, acoustic imaging by means of ballistic phonons should be performed preferably at low temperatures where the phonon mean free path is relatively long. Recently, the technique of electron beam scanning and laser beam scanning has been extended to the temperature range of liquid helium. Detailed reports on the experimental procedures can be found elsewhere [5,6,10,13].

The average energy of a phonon emitted from a region at temperature T is approximately given by:

$$\hbar\omega = k_B T \qquad (5)$$

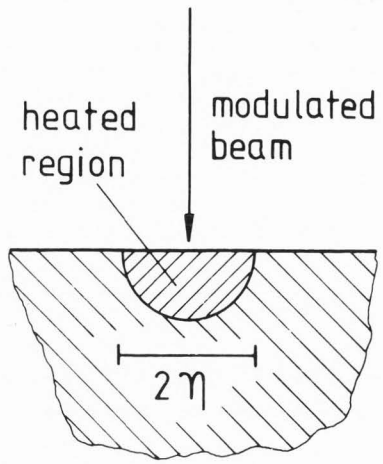

Fig. 1: Principle of scanning acoustic microscopy.

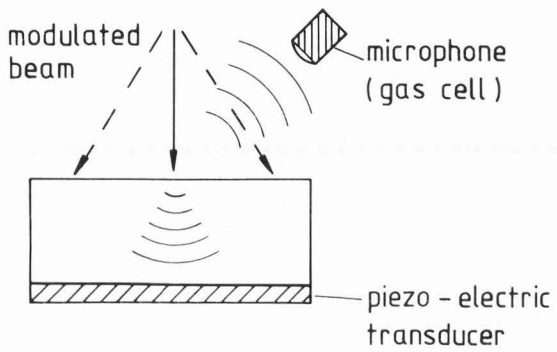

Fig. 2: Signal detection in scanning acoustic microscopy.

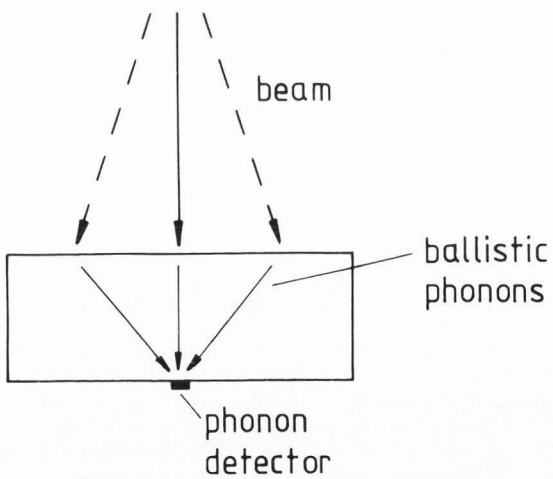

Fig. 3: Acoustic imaging based on the propagation of ballistic phonons.

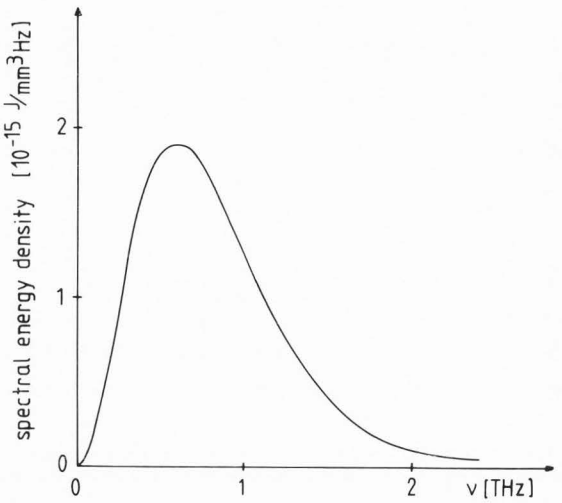

Fig. 4: Frequency dependence of the spectral energy density $u(\omega,T)$ after subtraction of the zero-point energy. (T = 10 K; v_s = 4000 m/s).

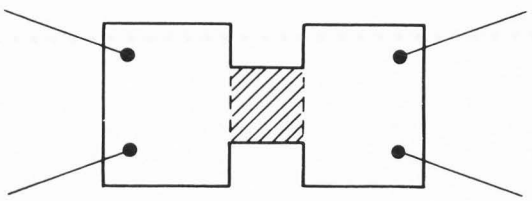

Fig. 5: Shape of a typical thin-film superconducting bolometer. The hatched part shows the effective bolometer area which can be as small as several μm^2.

Here $\hbar$ is Planck's constant divided by 2π, ω is the angular frequency of the phonon, and k_B is Boltzmann's constant. As an example, for T = 10 K we find from Eq. (5) the phonon frequency $\nu = \frac{\omega}{2\pi}$ = 0.208 THz. The wavelength λ of a phonon of such frequency in a typical metal is approximately $\lambda \approx 0.02$ μm.

The arrangement for acoustic imaging based on ballistic phonons is shown schematically in Fig. 3. The ballistic phonons originate from a localized region near the top surface of the sample at the coordinate point of the beam focus. They are detected by a localized phonon detector attached to the bottom surface of the sample. By scanning the beam over the top sample surface, ballistic phonons approaching from the different directions are recorded by the detector. The high spatial resolution required in this scheme can easily be accomplished using a phonon detector with very small area. Such small-area detectors can be obtained using standard microfabrication techniques. In addition to the high spatial resolution of the phonon detector, high temporal resolution can become necessary. We discuss these aspects of the phonon detector in more detail in

the following section.

The approximate value of the phonon frequency given in Eq. (5) directly results from the application of Planck's radiation law to the spectral energy density $u(\omega,T)$ of the phonons emitted from a region at temperature T [1]. According to Planck's law, the spectral energy density $u(\omega,T)$ is given by:

$$u(\omega,T) - u(\omega,0) = \frac{3\cdot\hbar\omega^3}{2\cdot\pi^2 v_s^3 (e^{\hbar\omega/k_B T}-1)} \quad . \qquad (6)$$

Here the second term on the left takes into account the zero-point energy. The factor $1/v_s^3$ is the average of the inverse third power of the long-wavelength phase velocities of the three acoustic phonon modes. The frequency dependence of expression (6) for the temperature T = 10 K is shown in Fig. 4. Here we have taken the value $v_s = 4000$ m/s for the sound velocity. The spectral energy density is seen to reach a maximum at some frequency ω_{max}. From Eq. (6) one obtains the relation

$$\hbar\omega_{max} = 2.82\ k_B T \quad . \qquad (7)$$

This represents a more accurate result than the approximation of Eq. (5). The result of Eq. (7) can also be written in the form:

$$\lambda_{max} \cdot T = 6.81 \cdot 10^{-8}\ m\cdot K \quad , \qquad (8)$$

where λ_{max} is the wavelength corresponding to the frequency ω_{max}. In the optical case relation (8) is known as Wien's displacement law.

In our discussion so far we have tacitly assumed that the region acting as phonon source is in thermodynamic equilibrium at the elevated temperature T. However, the beam irradiation results in a pronounced nonequilibrium configuration in this region. The primary processes due to the beam irradiation generate highly excited electrons which subsequently thermalize quickly via inelastic electron-electron and electron-phonon interactions. The typical time scale of these processes is about 10^{-12} s [6]. After this time the irradiated sample region can be thought to be in quasi-equilibrium at an effective temperature T^*. In this approximation the nonequilibrium distribution of the electrons and the phonons is described only by the value of T^*. In the following we adopt such a simplified picture in terms of the T^*-model and the concept of an effective temperature T^* of the region at the coordinate point of the beam focus. Such an approximation can be applied both for electron beam and laser beam irradiation. In the last section we show how the value of T^* can be estimated using arguments based on the expression in Eq. (6) and the Stefan-Boltzmann radiation law.

Space- and Time-Resolved Phonon Detection

From the scheme presented in Fig. 3 it is clear that the area of the phonon detector should be as small as possible in order to obtain maximum angular resolution. If the acoustic imaging is performed at a sample temperature in the range of liquid helium, highly sensitive devices such as superconducting bolometers or superconducting Josephson tunnel junctions can be used for phonon detection. The shape of a typical thin-film superconducting bolometer is shown in Fig. 5. The bolometer constitutes a superconducting microbridge placed between wide film sections at both ends for attaching current and voltage leads. If it is current-biased close to its superconducting transition temperature T_c, its voltage drop becomes highly sensitive to small amounts of energy deposited by the incoming phonons. Usually, the bolometer film is only a few hundred Å thick and is attached to the sample surface by vacuum deposition and standard lithographic techniques. Recently, we have fabricated superconducting bolometers from O_2-doped aluminum films with 400 Å thickness and an effective area as small as 2 µm x 2 µm. The critical temperature of these bolometers was 1.7 K. Further details about the operation of such bolometers can be found elsewhere [5].

In addition to superconducting bolometers and Josephson tunnel junctions, thin-film piezoelectric transducers appear feasible for high-sensitivity phonon detection. Using standard microfabrication techniques, dimensions of the effective detector area as small as about 1 µm x 1 µm can be achieved. Of course, beside the dimensions of the phonon detector, the extent of the heated region acting as the phonon source is highly crucial for determining the angular resolution limit of the acoustic imaging process. We come back to this influence of the phonon source at the end of this paper.

In addition to the high spatial resolution of the phonon detector, high time resolution is also required. The thermal relaxation time τ_α of a thin-film bolometer attached to the specimen is given by:

$$\tau_\alpha = \frac{\rho \cdot c \cdot d}{\alpha} \quad . \qquad (9)$$

Here d is the thickness of the bolometer film and α the heat transfer coefficient accounting for the energy transfer from the film into the substrate. For an O_2-doped aluminum film of 400 Å thickness at 1.7 K and using a value $\alpha = 0.1\ Wcm^{-2}K^{-1}$ we obtain from Eq. 9 the typical value $\tau_\alpha = 6.4 \cdot 10^{-10}$ s. From this we see that such a bolometer is suitable for detecting the modulated phonon flux generated by modulated beam irradiation of the sample up to modulation frequencies of about 1.6 GHz.

Phonon Focusing

As the first example of acoustic imaging using the ballistic phonons emitted from the region locally heated by the electron beam, we briefly discuss the phenomenon of phonon focusing in a single crystal. Due to the anisotropy of the elastic constants of a single-crystalline material, the phonon energy flux through the crystal shows distinct anisotropy. In fact, along certain crystallographic directions (corresponding to the inflection points on the surface of constant phonon energy in wavevector space) the phonon energy flux can diverge. For detecting this anisotropy of the phonon energy flux, a crystal geometry

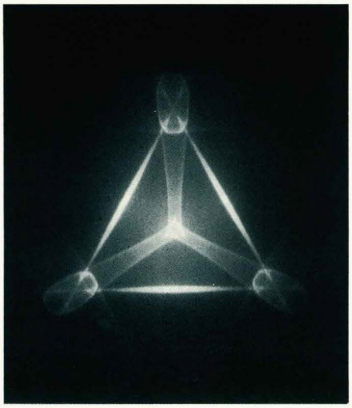

Fig. 6: Two-dimensional image of the anisotropic energy flux of ballistic phonons in single-crystalline [111]-oriented silicon. For further details see text.

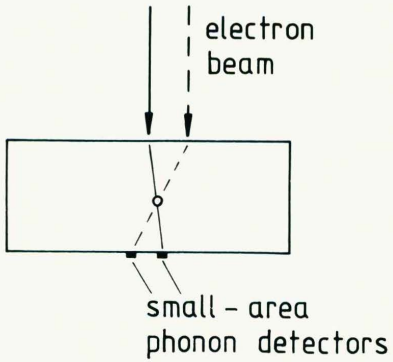

Fig. 8: Principle of the three-dimensional acoustic imaging of an object (indicated by the circle) which scatters or absorbs the ballistic phonons. Due to the position of the object, the signal of the two phonon detectors shown at the bottom is affected for different positions of the electron-beam focus during the scanning process.

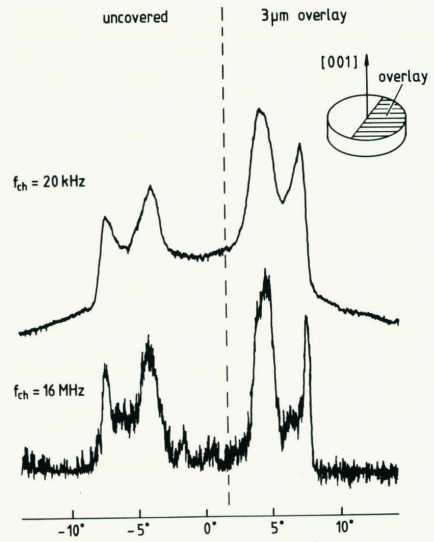

Fig. 7: Bolometer signal from a linear scan over the (001) surface plane of a [001] oriented Ge single crystal. Half of the scanned surface is covered with a 3-µm overlay film of O_2-doped Al as shown on the inset. Further details are given in the text.

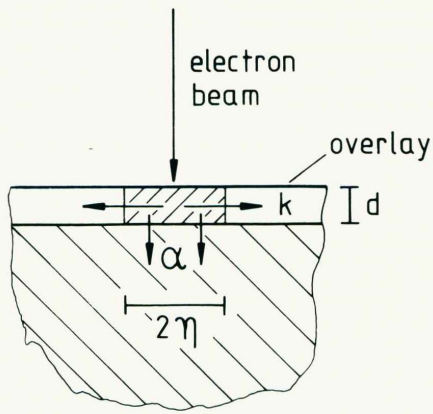

Fig. 9: Overlay geometry for improving the spatial resolution of acoustic imaging. The electron-beam energy dissipated in the overlay film of thickness d is conducted away by heat conduction within the overlay film (heat conductivity k) and by heat transfer across the bottom surface of the overlay film (coefficient α).

with two flat surfaces running parallel to each other is preferable. By scanning one surface with the beam, the phonons propagating through the crystal are detected using a small-area bolometer attached to the opposite surface. By recording the bolometer signal as a function of the coordinates of the beam focus, the anisotropy of the phonon energy flux can be measured. Recently such experiments have been performed with single-crystalline α-quartz, sapphire, germanium,and silicon using electron-beam scanning at liquid-helium temperatures. In Fig. 6 we show the two-dimensional

image of the anisotropic energy flux of ballistic phonons in single-crystalline silicon. The sample is a disk of 20 mm diameter and 2 mm thickness. The [111] direction is oriented perpendicular to the plane of the figure. Bright regions indicate high intensity of the phonon flux. The scanned area shown is 7 mm x 8 mm, corresponding to an angle of about $\pm$ 60° around the [111] axis. The image shown in Fig. 6 represents the time-integrated bolometer signal. This signal is proportional to the total phonon intensity, i.e., to the sum of the different acoustic phonon branches.

Employing time-resolved phonon detection, the anisotropic propagation of the different acoustic phonon modes could be observed separately. Further details can be found in a series of recent reports [5, 6, 7, 9].. Using laser-beam scanning at liquid-helium temperatures, Wolfe and Northrop have performed similar experiments, mostly concentrating on Ge and GaAs [10, 14].

Recently we have carried out a series of experiments designed to clarify the angular resolution obtained in phonon focusing measurements by electron-beam scanning at liquid-helium temperatures. For the experiments we have used a high-purity single-crystalline disk of Ge with 20 mm diameter, 3.0 mm thickness, and [001] orientation in axial direction. The nominal sample purity was $N_D - N_A \approx 1 \cdot 10^{10} cm^{-3}$, N_D and N_A being the donor and acceptor concentration, respectively. The bolometer, attached to the bottom surface of the Ge disk near its center, was fabricated from O_2-doped Al. It had a thickness of 400 Å and an effective area of 2 µm x 2 µm. The measurements were done at a temperature of 1.7 K. In Fig. 7 we show a plot of the bolometer signal obtained from a linear scan over the (001) surface plane, the direction of the scanning line being parallel to the (011) plane. The angles given in Fig. 7 denote the angle between the [001] direction and the direction of the phonon energy flux within the corresponding plane. Without going into the detail of the geometric pattern of phonon focusing in [001] oriented Ge, we will concentrate only on two points displayed by the plots in Fig. 7. First we note that the two peaks on the left (negative angles) are considerably smaller than the two peaks on the right (positive angles). This non-symmetry results from the fact that for the positive angles the Ge surface to be irradiated carried an overlay film of O_2-doped Al of 3 µm thickness, whereas for the negative angles the Ge surface remained uncovered (see inset of Fig. 7). The reduction in the bolometer signal for the uncovered part of the Ge crystal can be explained by the larger electron backscattering coefficient in Ge compared to Al. Therefore, the electron beam energy deposited in the sample is larger in the part covered with Al than in the uncovered part. At the end of this paper we return to the possibilities for improving the spatial resolution of acoustic imaging by properly chosen overlays attached to the specimen surface to be irradiated.

The second point we note from Fig. 7 is the strong influence of the modulation frequency of the beam upon the angular resolution. Clearly, the lower trace obtained at the modulation frequency of 16 MHz shows much sharper contours than the upper trace obtained at 20 kHz. Qualitatively, such behavior is expected from Eq. (1) or (4).

Turning now to the sharp peak at the far right on the lower trace of Fig. 7, it can serve for providing us with an upper-limit-estimate of the effective diameter of the phonon source as detected by the high-frequency signal. From the steep slope on the right of this peak and the flight path of the phonons between source and detector, the effective diameter is estimated not to exceed about 25 µm. We note that the 2 µm extent of the bolometer is relatively small compared to this value. For the sample thickness of 3 mm an effective diameter of the phonon source of 25 µm corresponds to an angular resolution of about 0.48°. We note that these values refer to the signal modulated at 16 MHz. On the other hand, the diameter of the region heated by the electron beam is found from the measurements at low modulation frequencies. From the upper trace in Fig. 7 (obtained at 20 kHz modulation frequency) this diameter is estimated not to exceed about 60 µm.

Three-Dimensional Acoustic Imaging

The ballistic phonons emitted from a localized phonon source at the specimen surface also can serve for acoustic imaging of inhomogeneities in the interior of the sample such as precipitates, voids, doping structures, etc. For this, phonon detection with high spatial resolution again will be crucial. The principal scheme is shown in Fig. 8. Here one utilizes the attenuation of the detector signal due to the scattering or absorption of the ballistic phonons by an object placed along the path connecting the source and the detector. By proper arrangement of two or more detectors, three-dimensional acoustic imaging becomes possible using the different detector signals recorded during the scanning process (tomography principle). If the detectors are placed far apart from each other, a large section of the specimen can be investigated in this way. On the other hand, if the number of objects per unit volume to be detected is large, it becomes possible that more than one object causing scattering or absorption can be found along the path connecting source and detector. An unambiguous interpretation of the detector signal then becomes difficult or impossible. Therefore, it can be advantageous to place the different detectors relatively close to each other. In this case the inspection is restricted to a relatively small sample section.

Of course, the spatial resolution of this technique is again limited by the area of the source and of the detector. The depth range for probing the sample interior is limited by the phonon mean free path l_{ph}. Therefore, the method is applied preferably at low temperatures, where l_{ph} can be as large as several mm or more.

Regarding the characteristic time scales we note that the time of flight of ballistic phonons for typically a 3 mm distance between source and detector and a sound velocity of 3000 m/s is 1 µs. This time is much shorter than the typical time scale of the scanning process. As an example we take a 3 mm x 3 mm surface area and a total

scanning time of 2 min. For a 10 μm x 10 μm area element on the sample surface, this corresponds to an exposure time of about 1 ms. In order to select the bolometer signal from the individual acoustic phonon modes and for improving the spatial resolution of the imaging process, time-resolved detection of the bolometer signal can become necessary. Here a time resolution of about 10 ns appears quite feasible [5].

According to Eq. (7) the wavelength of the dominant phonons emitted from a region heated to 10 K by the electron beam, is as small as about 0.01 μm. (Here we have assumed that except for the irradiated region the sample temperature is in the liquid-helium range). Because of such a small phonon wave length, we can treat the acoustic imaging of objects with dimensions in the range of 1 μm or larger using the concepts of geometrical optics. In this case the acoustic image detected by the bolometers just represents the "shadow" caused by the object.

Resolution Estimate

As we have seen above, the spatial resolution limit of the acoustic imaging method appears to be dominated by the extent of the localized heated region acting as the phonon source, since the effective area of the phonon detectors can be made very small (say, 1 μm x 1 μm) by standard microfabrication techniques. The resolution limit is then given by the length η of Eq. (1) or (4). From Eq. (4) we note that the mean free path l (of the electrons and/or the phonons, depending upon the type of material) becomes crucial. This dependence upon l would suggest to perform the acoustic imaging at room temperature or higher temperatures, where the mean free path is very small. However, at or above room temperature the penetration depth of the ballistic phonons (given by the phonon mean free path l_{ph}) is also very small, rendering the operation at room temperature impractical. Clearly, for obtaining a large range of penetration of this acoustic imaging method, operation in the temperature range of liquid helium (where l_{ph} is large) is highly advantageous.

Taking the Ge sample discussed above and the results shown in Fig. 7 as an example, we calculate from the thermal sample properties the value $\eta \approx 250$ μm using Eq. (1) and taking the frequency $\nu = 16$ MHz. Here the heat conductivity k and the specific heat C of Ge were evaluated (using tabulated values) at the liquid-helium bath temperature of 1.7 K, at which our experiments had been performed. The value of η obtained in this way is by far larger than the upper-limit estimate based on the sharp outer peaks shown in the lower trace of Fig. 7. Looking at the peak on the far left, corresponding to the uncovered part of the Ge sample, we estimate from its steep slope on the left and the 3 mm flight path of the phonons between source and detector, that the effective diameter of the phonon source cannot exceed about 25 - 30 μm. The large discrepancy between both values of the effective source diameter must be due to the fact, that in our estimate based on Eq. (1) we have ignored the localized heating effect caused by the beam irradiation. Due to this temperature rise, the mean free path of the phonons and of the charge carriers (generated by the beam irradiation) will be reduced considerably, leading to a strong reduction of the length η, as seen from Eq. (4).

We note that after leaving the heated source region, the phonons encounter a sample temperature close to that of the low-temperature bath, at which their mean free path is very long.

A rough estimate of the effective temperature in the localized region acting as phonon source can be obtained in the following way. We assume that the electron-beam power dissipated in the sample is completely removed via the emission of the ballistic phonons. The power emitted by the phonons from a region at temperature T^* into the half-space adjoining this region is given per unit area by

$$P_{phonon} = \frac{v_s}{4} w(T^*) \quad , \tag{10}$$

where v_s is the sound velocity (averaged over the different acoustic modes) and $w(T^*)$ the density of the phonon energy in this region. The energy density $w(T^*)$ is found from the spectral energy density $u(\omega,T^*)$ of Eq. (6) by integration over all phonon frequencies, yielding

$$w(T^*) = \frac{1}{10} \pi^2 \frac{(k_B T^*)^4}{(\hbar v_s)^3} \quad . \tag{11}$$

The relation stated in Eqs. (10) and (11) is known as the Stefan-Boltzmann law in the optical case. As an example we take our experimental results for the Ge sample discussed above and shown in Fig. 7. Here the power of the electron beam was 26 mW. Assuming the value of 60 μm x 60 μm estimated above in the low-frequency limit for the effective area of the phonon source and taking about 80 % of the beam power as the fraction dissipated in the sample, we find from Eqs. (10) and (11) by balancing the power

$$\frac{v_s}{4} \cdot \frac{\pi^2}{10} \frac{(k_B T^*)^4}{(\hbar v_s)^3} = \frac{20 \text{ mW}}{3600 \text{ μm}^2} \quad . \tag{12}$$

Taking $v_s = 3500$ m/s for the average sound velocity in Ge, we calculate from Eq. (12) the value $T^* \approx 10$ K for the effective temperature of the phonon source. Of course, a rough estimate of T^* can also be obtained in principle from a more quantitative analysis of the expected temperature dependence of the length η together with experimental data such as shown in Fig. 7.

Finally, we compare the results shown in Fig. 7 for positive and negative angles, i.e., for the section of the Ge sample covered with a 3 μm thick overlay from O_2-doped Al and for the uncovered section, respectively. For the sample section covered with the Al overlay we have calculated above an effective diameter of the phonon source of about 25 μm. A similar value was obtained for the uncovered section.

In certain cases the metal-film overlay can be expected to result in an appreciable improvement of the spatial resolution. If the dominant part of the beam energy is dissipated in the metal-film overlay, the overlay material will determine

the effective radius η of the phonon source. Therefore, the application of a metallic overlay film with a small mean free path l of the electrons and the phonons can be an interesting way for improving the spatial resolution. Recently, we have systematically investigated the spatial spreading of the thermal perturbation due to electron-beam irradiation in various superconducting Pb-alloy film overlays on sapphire substrates [11]. This overlay geometry is shown schematically in Fig. 9. The effective radius η of the heated region in the overlay film is given by [11]:

$$\eta = \frac{\eta_o}{\{\frac{1}{2}(\sqrt{1+(\frac{\omega}{\omega_c})^2}+1\}^{1/2}} \quad . \tag{13}$$

Here η_o is the static thermal healing length:

$$\eta_o = (\frac{k \cdot d}{\alpha})^{1/2} \quad , \tag{14}$$

where k and d are the heat conductivity and the thickness of the overlay film, respectively, and α is the heat transfer coefficient between the overlay film and the substrate. The critical frequency ω_c is given by:

$$\omega_c = \frac{\alpha}{\rho \cdot C \cdot d} \tag{15}$$

and is the inverse of the thermal relaxation time τ_α of Eq. (9). The quantities ρ and C are the mass density and the specific heat of the overlay film, respectively. In the limit $\omega >> \omega_c$ Eq. (13) yields $\eta = (\frac{2k}{\rho \cdot C \cdot \omega})^{1/2}$, i.e., the same result as Eq. (1). Equation (13) refers to the spatial spreading of the temperature modulation when the beam power is modulated at angular frequency ω. Of course, in order to utilize the increase in resolution with increasing frequency ω, the modulated signal must be detected. The unmodulated part of the heated region extends up to the distance η_o given by Eq. (14). We note that the dynamic thermal healing length η is identical to the characteristic length scale appearing in thermal wave microscopy.

By varying the modulation frequency between 100 kHz and 18 MHz, the frequency dependence of η predicted from Eq. (13) has been experimentally confirmed [11]. From these results it appears that an effective diameter of the phonon source as small as about 1 µm can be obtained for sample temperatures in the liquid-helium range and for a modulation frequency between 10 and 100 MHz, if a suitable metal-film overlay is applied to the specimen.

Conclusions

The established concepts of scanning electron-acoustic and photo-acoustic microscopy utilize as the carrier of information the acoustic wave generated at the same frequency (or some harmonics) as the modulation frequency of the beam irradiation. The thermal and elastic property information obtained from this principle is restricted to a region close to the sample surface, the depth of penetration being in the order of 1 µm. On the other hand, acoustic information on structural properties (subsurface cracks etc.) can be obtained for depths of several hundred µm. In a different principle, the ballistic phonons emitted from the localized region heated by the beam irradiation can be utilized for acoustic imaging. If the sample is cooled to temperatures in the range of liquid helium, the ballistic phonons can propagate over distances as large as several mm and, therefore, can probe sample inhomogeneities even relatively far away from the surface. The frequency distribution of the ballistic phonons can be obtained from Planck's radiation law in good approximation. For a temperature of the phonon source of 10 K the dominating phonon frequency is about 0.6 THz. In this new concept for acoustic imaging, highly localized phonon detectors become crucial. Using two or more phonon detectors simultaneously during the scanning process, three-dimensional acoustic imaging becomes possible. Using standard microfabrication techniques, phonon detectors with an effective area of about 1 µm x 1 µm can be realized. The spatial resolution limit of this imaging method then appears to be dominated by the effective diameter of the region heated by the beam and acting as the phonon source. Using proper overlay films for dissipating the beam energy, a spatial resolution limit in the range of 1 µm appears feasible.

Acknowledgements

Financial support of this work from a grant of the Deutsche Forschungsgemeinschaft is gratefully acknowledged. The authors would like to thank P. Glasow, Siemens, Erlangen, for kindly supplying the Ge specimen. This paper was written by one of the authors (R.P.H.) during a visit to the Electrotechnical Laboratory, Sakura-mura, Ibaraki, Japan. He would like to thank Dr. H. Hayakawa and the members of the Cryoelectronics Section for their kind hospitality. Stimulating discussions with Dr. T. Ishiguro and Dr. K. Kajimura are also gratefully acknowledged.

References

1. Ashcroft NW, Mermin ND. (1976). Solid State Physics, Holt, Rinehart and Winston, New York.

2. Balk LJ, Kultscher N. (1983). Scanning Electron Microscopy. Beitr. elektronenmikroskop. Direktabb. Oberfl., Verlag Remy, Münster, BEDO 16, 107-120.

3. Balk LJ, Davies DG, Kultscher N. (1984). Application of Nonlinear Scanning Electron Acoustic Microscopy in Metals Research, Scanning Electron Microsc. 1984;IV:1601-1610.

4. Cargill GS. (1980). Electron-Acoustic Microscopy, in: Scanned Image Microscopy, EA. Ash (ed), Academic Press, New York, p. 319-330.

5. Eichele R, Huebener RP, Seifert H. (1982). Phonon Focusing in Quartz and Sapphire Imaged by Electron Beam Scanning. Z. Phys. B48, 89-97.

6. Huebener RP. (1984). Applications of Low-Temperature Scanning Electron Microscopy. Rep. Prog. Phys. 47, 175-220.

7. Huebener RP, Seifert H. (1984). Applications of Low-Temperature Scanning Electron Microscopy. Scanning Electron Microsc. 1984; III: 1053-1063.

8. Luukkala M. (1980). Photoacoustic Microscopy at Low Modulation Frequencies, in: Scanned Image Microscopy, EA. Ash (ed). Academic Press, New York, p. 273-289.

9. Metzger W, Eichele R, Seifert H, Huebener RP. (1984). Phonon Focusing in Germanium Imaged by Electron-Beam Scanning, in: Phonon Scattering in Condensed Matter. W. Eisenmenger, K. Laßmann, S. Döttinger (ed.), Springer, Berlin, p. 72-74.

10. Northrop GA, Wolfe JP. (1980). Ballistic Phonon Imaging in Germanium. Phys. Rev. B22, 6196-6212.

11. Pavlicek H, Freytag L, Seifert H, Huebener RP. (1984). Resolution Limit Due to Thermal Effects in Low-Temperature Scanning Electron Microscopy. J. Low Temp. Phys. 56, 237-257.

12. Rosencwaig A. (1980). Thermal-Wave Imaging and Microscopy, in: Scanned Image Microscopy. EA.Ash (ed). Academic Press, New York, p. 291-317.

13. Seifert H. (1982). Liquid Helium Cooled Samplestage for Scanning Electron Microscope. Cryogenics 22, 657-660.

14. Wolfe JP, Northrop GA. (1984). Search for Large k-Vector Phonons in GaAs, in: Phonon Scattering in Condensed Matter, W. Eisenmenger, K. Laßmann, S. Döttinger (ed.), Springer, Berlin, p. 100-102.

15. Wong YH. (1980). Scanning Photo-Acoustic Microscopy, in: Scanned Image Microscopy, EA. Ash (ed), Academic Press, New York, p. 247-271.

Discussion with Reviewers

D.G. Davies: How are the low temperature, beam modulated experiments essentially different from conventional SEAM?
Authors: In both cases a thermal wave is generated at the specimen surface due to the irradiation with the modulated beam. In SEAM one utilizes the acoustic wave generated at the angular frequency ω of the beam modulation. This acoustic wave only consists of phonons of frequency ω generated coherently. In our low temperature experiments based on the ballistic phonon signal, the phonons are emitted incoherently from the heated location and their frequency distribution is given by Planck's radiation law. Here the beam modulation is not an essential ingredient of the phonon generation process. It only serves for employing more sensitive techniques for signal detection and for reducing the diameter of the region from which the modulated ballistic phonon flux originates. Since in our experiments the phonon frequencies extend up to the THz range, attenuation of the ballistic phonons in the specimen is very strong, unless the sample is cooled to the temperature range of liquid helium. In addition, the fact that we use localized, small-area phonon detectors, represents a distinct feature of our experimental scheme.

W.L. Holstein: You deal exclusively with thermally generated ballistic phonons. Can ballistic phonons also be generated directly from the electron beam through electron-phonon interactions?
Authors: The microscopic mechanism by which the energy transfer takes place from the electron beam to the specimen (excitation of phonons, charge carriers, etc) is highly complex. This complexity is particularly striking if we look at the primary processes taking place within a time scale of 1 ps or less upon impact of the electron beam. Eventually, on a longer time scale of the order of 1 ns, all these primary processes result in a localized heating effect. We simply ignore the initial sub ps period and concentrate on the time scale where a description in terms of localized heating is applicable. In various experiments reported elsewhere we have shown that such a simplified treatment is justified.

W.L. Holstein: In three-dimensional acoustic imaging for the detection of voids in the interior of a material, what limits are placed on the specimen? Must it be a single crystal? Must it be polished?
G.S. Cargill: Is this technique applicable only to single crystals? What limitations on mean free path are expected when examining polycrystals, ceramics, metals, glasses?
Authors: The prime requirement for this acoustic imaging is a long mean free path of the ballistic phonons. Therefore, in addition to the low-temperature operation, the absence of a high concentration of defects, which reduce the phonon mean free path, is required. How grain boundaries affect the ballistic phonon signal remains to be seen. Regarding the treatment of the specimen surface scanned by the electron beam we must note that a highly irregular surface already results in a variation of the ballistic phonon signal with the coordinates of the beam focus. Therefore, the sample surface to be scanned must be polished.

L.J. Balk: You only consider phonon production due to heating of the sample. At normal temperatures a primary electron of, say 30 keV, produces about 10^4 electron-hole-pairs. These recombine to a considerable percentage via nonradiative processes and, by this, additional phonon production occurs. Furthermore, the local correlation of the phonon production to the beam entry point is influenced by the diffusion length of minority carriers. How is this effect to be considered at liquid helium temperatures?
Authors: These are interesting questions. They refer again to the primary processes and to the point raised by Holstein. The diffusion length of minority carriers clearly must be included in a discussion of the effective diameter of the phonon source. R. Groß and M. Koyanagi of our group have recently analyzed this problem for thin-film superconductors deposited on a substrate. An analysis for semiconductors remains to be done.

L.J. Balk: How small can the detectors be made without affecting the signal-to-noise ratio? Is signal-to-noise no problem in your technique, which might influence either the spatial and angular resolution or the recording time?

Authors: So far our smallest detectors had an area of 2 μm x 2 μm. In our experiments on phonon focusing the signal-to-noise ratio did not present any problem. Systematic experiments on the limitations imposed by the signal-to-noise ratio upon the resolution of the three-dimensional acoustic imaging of structural inhomogeneities are presently under way.

L.J. Balk: The active radius of the phonon source is certainly affected by the primary electron energy used and should be smaller with lower energy due to a change dissipation volume of this primary energy. This effect is to a first approximation quadratic and thus not only the volume should decrease significantly, additionally the heat deposition density should increase. Therefore at low primary electron energy there should still be enough signal available. Could you comment on this, and what was the primary electron energy you used? Would lowering the primary energy yield the same effect like the overlay technique you propose?
Authors: Our primary electron energy was typically 26 keV. Recent experiments on phonon focusing in single-crystalline germanium performed in the range of beam energies between 5 and 26 keV have indicated that the beam energy did not significantly influence the spatial resolution.

N. Kultscher: You mention the necessity of a long phonon mean free path for the acoustic imaging. Furthermore you show that the mean free path is shorter in the heated region near the surface of the sample. Does this short mean free path produced in the heated area complicate the interpretation of the contrast due to scattering mechanisms already close to the surface? Can you determine experimentally that a signal change is only due to propagation of phonons and not to a changed phonon production at the heated sample point?
Authors: The interpretation of the contrast in terms of structural properties affecting only the phonon propagation becomes unambiguously clear if the ballistic phonon signal is recorded simultaneously with two different detectors located a short distance apart from each other. In this way the discrimination between contrast due to the generation process and that due to the propagation process of the ballistic phonons is straightforward, as we have demonstrated in recent experiments.

N. Kultscher: You only considered an averaged effective temperature model as a result of a thermodynamical viewpoint on energy relaxation of the highly excited electrons in the heated region. How would the interpretation change, if one takes into account the energy density distribution in the primary beam and thus in the heated region, too, which is still present even after the energy relaxation? And how is the imaging process affected by the generated distribution of the phonon energies and thus phonon frequencies?
Authors: So far we have only considered an effective diameter of the region acting as a source for the ballistic phonons and have ignored any lateral spatial structure within the source. The frequency distribution of the ballistic phonons is expected to influence their attenuation since the phonon scattering rates strongly increase with increasing phonon frequency.